Chapter 10

Monte Carlo Calculations of Light Scattering by Large Particles with Multiple Internal Inclusions

Andreas Macke
Institut für Meereskunde
24105 Kiel, Germany

I. INTRODUCTION

The difficulty of calculating the scattering of electromagnetic radiation by many naturally occurring particles is due to a large extent to their nonsphericity, but is also attributable to inhomogeneities within the particles. Examples in remote-sensing and climatology studies are water droplets in the terrestrial atmosphere that contain various insoluble inclusions, ice particles with internally trapped air bubbles, inhomogeneous composites of mineral aerosols, and planetary regolith particles. Internal scattering also complicates the optical techniques for material testing. Examples are the detection of contamination on silicon wafer

Light Scattering by Nonspherical Particles: Theory, Measurements, and Applications

surfaces (Ivakhnenko *et al.*, 1998) or the optical particle sizing in industrial spray drying of food (Göbel *et al.*, 1997).

The calculation of the scattering properties of particles with arbitrary shapes and internal structures is rather difficult. Exact solutions exist for a few symmetric particles with layered structures (e.g., Toon and Ackerman, 1981) as well as for spherical particles with arbitrarily located spherical inclusions (Fuller, 1995b; Chapters 8 and 9). Furthermore, a number of algorithms based on the discrete dipole approximation (Purcell and Pennypacker, 1973; Chapter 5) have been developed to treat scattering by nonspherical particles with arbitrary internal optical structures (Goedecke and O'Brien, 1988). However, the relatively high demands for computer time and memory limit applications of these techniques to moderate size parameters.

In this chapter, a relatively simple hybrid technique combining ray optics and Monte Carlo radiative transfer is presented, which permits the treatment of light scattering by arbitrarily shaped host particles containing spherical and nonspherical inclusions and is valid for host particles that are large compared to the wavelength of the incoming radiation. It, therefore, extends the treatment of nonspherical, inhomogeneous particles to the large size parameter range.

Section II describes the ray-tracing/Monte Carlo model. Applications to light scattering by atmospheric ice crystals and lunar soil grains are discussed in Section III. A simplified treatment of the scattering problem using an independent superposition of the scattering properties of the host and internal particles is presented in Section IV. Finally, some concluding remarks and a brief outline of further potential applications are given in Section V.

II. RAY-TRACING/MONTE CARLO TECHNIQUE

The scattering of a light ray entering a particle containing discrete inclusions is simulated by a combination of ray-tracing and Monte Carlo techniques (hereafter referred to as the RT/MC technique). The ray-tracing program takes care of the individual reflection and refraction events at the outer boundary of the particle (e.g., Muinonen *et al.*, 1989; Chapters 11 and 15) and the MC routine simulates internal scattering processes.

After an incident photon is refracted into the host particle, it is allowed to travel a free path length l given by

$$l = -\bar{l} \log R(0, 1), \tag{1}$$

where $\bar{l}$ is the mean free path length between two subsequent scattering events and $R(0, 1)$ is an equally distributed random number within the interval $(0, 1)$.

If the photon has not reached one of the boundaries of the medium, its previous direction is changed along the local zenith Θ and azimuth φ scattering angles

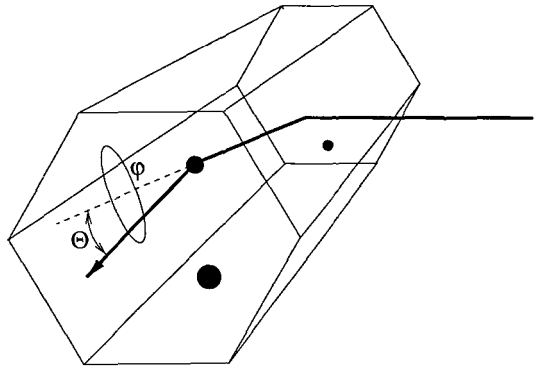

Figure 1 Illustration of the internal scattering geometry in hexagonal ice crystal with inclusions.

(Fig. 1) according to

$$\int_0^{\Theta} a_1^{\text{incl}}(\Theta') \sin\Theta' \, d\Theta' = R(0,1) \int_0^{\pi} a_1^{\text{incl}}(\Theta') \sin\Theta' \, d\Theta', \tag{2}$$

$$\varphi = R(0, 2\pi), \tag{3}$$

where a_1^{incl} denotes the scattering phase function (Section XI of Chapter 1) of the internal scatterer. Absorption is taken into account by multiplying the photon energy with the single-scattering albedo ϖ^{incl} of the internal scatterer. Together with the processes described by Eqs. (1)–(3), this represents a direct Monte Carlo solution of the radiative transfer equation for a scattering and absorbing medium. These processes are repeated until the photon enters the host boundary surface, where it is again subject to reflection and refraction events. The entire procedure is repeated again for the internally reflected component each time until the photon energy falls below a specified threshold.

Note that calculations of the internal scattering properties require a nonabsorbing surrounding host medium. However, absorption within the host medium can still be taken into account by adding purely absorbing inclusions.

The scheme outlined previously produces the ray-tracing single-scattering albedo ϖ^{RT} and the ray-tracing scattering phase function a_1^{RT} for the host particle. Additionally, diffraction on the host particle's projected area S must be taken into account. For polyhedral particles, the projected area can be described by a closed polygon, from which the diffraction phase function a_1^{D} can be calculated analytically (Cai and Liou, 1982; Macke *et al.*, 1996b). For large spherical host particles with size parameters $x = 2\pi r/\lambda \gg 1$, diffraction is given by

(van de Hulst, 1957)

$$a_1^{\mathrm{D}}(\Theta) = \begin{cases} 4x^2\left(\dfrac{J_1(x\sin\Theta)}{x\sin\Theta}\right)^2, & \Theta \in \left[0, \dfrac{\pi}{2}\right], \\ 0, & \text{otherwise}, \end{cases} \tag{4}$$

where $J_1(y)$ is the Bessel function of the first kind, r is the particle radius, and λ is the wavelength.

Ray-tracing and diffraction properties are added, weighted by their individual scattering cross sections. By definition, the ray-tracing extinction cross section is equal to the geometric cross section of the host particle, $C_{\mathrm{ext}}^{\mathrm{RT}} = S$, and the ray-tracing scattering cross section is equal to $C_{\mathrm{sca}}^{\mathrm{RT}} = \varpi^{\mathrm{RT}} S$. The diffraction extinction cross section $C_{\mathrm{ext}}^{\mathrm{D}} = S$ is always equal to the diffraction scattering cross section $C_{\mathrm{sca}}^{\mathrm{D}}$. Therefore, the total cross sections, single-scattering albedo, and phase functions are given by

$$C_{\mathrm{ext}} = C_{\mathrm{ext}}^{\mathrm{RT}} + C_{\mathrm{ext}}^{\mathrm{D}} = 2S, \tag{5}$$

$$C_{\mathrm{sca}} = C_{\mathrm{sca}}^{\mathrm{RT}} + C_{\mathrm{sca}}^{\mathrm{D}} = \left(1 + \varpi^{\mathrm{RT}}\right) S, \tag{6}$$

$$\varpi = \frac{C_{\mathrm{sca}}}{C_{\mathrm{ext}}} = \frac{\varpi^{\mathrm{RT}} + 1}{2}, \tag{7}$$

$$a_1(\Theta) = \frac{C_{\mathrm{sca}}^{\mathrm{RT}} a_1^{\mathrm{RT}}(\Theta) + C_{\mathrm{sca}}^{\mathrm{D}} a_1^{\mathrm{D}}(\Theta)}{C_{\mathrm{sca}}^{\mathrm{RT}} + C_{\mathrm{sca}}^{\mathrm{D}}} = \frac{\varpi^{\mathrm{RT}} a_1^{\mathrm{RT}}(\Theta) + a_1^{\mathrm{D}}(\Theta)}{\varpi^{\mathrm{RT}} + 1}. \tag{8}$$

The anisotropy of the scattered radiation is described by the asymmetry parameter

$$\langle\cos\Theta\rangle = \int_0^{\pi} a_1(\Theta)\cos\Theta\sin\Theta\, d\Theta = \frac{\varpi^{\mathrm{RT}}\langle\cos\Theta\rangle^{\mathrm{RT}} + \langle\cos\Theta\rangle^{\mathrm{D}}}{\varpi^{\mathrm{RT}} + 1}. \tag{9}$$

For large size parameters, the diffraction asymmetry parameter is very close to 1 so that

$$\langle\cos\Theta\rangle \approx \frac{\varpi^{\mathrm{RT}}\langle\cos\Theta\rangle^{\mathrm{RT}} + 1}{\varpi^{\mathrm{RT}} + 1}. \tag{10}$$

Note that the use of RT and MC techniques entails the following two assumptions. First, the distance between nearest neighbor internal scatterers must be larger than a few times their radii in order to treat them as independent scatterers. Second, the distance between the host particle boundary and internal scatterers must also exceed a certain value in order to assure the validity of Snell's law and Fresnel's formulas. According to Mishchenko *et al.* (1995), both conditions require a mean free path length $\bar{l}$ larger than about four times the radius of the internal scatterers. Therefore, even for a small number density of internal scatterers, the random nature of the Monte Carlo process will lead to occasional

violations of this requirement. However, setting $\bar{l}$ to 20 times the particles' radii ensures that possible near-field effects play only a minor role in the total scattering simulation.

It should be noted that this computational scheme in its present state does not include interference mechanisms such as coherent backscattering (Tsang *et al.*, 1985, Chapter 5; Barabanenkov *et al.*, 1991). This mechanism results from constructive interference of so-called self-avoiding reciprocal multiple-scattering paths and causes a narrow intensity peak centered at exactly the backscattering direction. Although coherent backscattering does not change the total optical cross section of the composite particle and is unlikely to modify noticeably the total asymmetry parameter, it may increase the total backscattering phase function by as much as 50–60% (Mishchenko, 1992b) and, therefore, can significantly affect the results of active remote-sensing retrievals such as lidar measurements.

III. RESULTS

The following two sections describe example applications of the RT/MC technique. Section A describes light scattering by inhomogeneous atmospheric ice crystals and is partly based on the paper by Macke *et al.* (1996a). The second example (Section B) examines the effect of internal structures on the asymmetry parameter of composite particles and summarizes the results derived by Mishchenko and Macke (1997).

A. Atmospheric Ice Particles

The study of light scattering by atmospheric ice crystals is largely motivated by the strong variability of ice particle shapes (e.g., Takano and Liou, 1995; Macke *et al.*, 1996b; Chapter 15). In most studies, the ice material itself is assumed to be homogeneous. In fact, although the shape problem is obvious from numerous *in situ* aircraft measurements (e.g., Heymsfield *et al.*, 1990), little is known about the internal structure of the ice particles. Considering the possible increase of the concentration of aerosol particles in the upper troposphere, caused either by natural phenomena such as volcanic eruptions (Sassen *et al.*, 1995) or by anthropogenic causes such as high-altitude aircraft exhausts (Schumann, 1994) or high-reaching convective transport of industrial combustions (Raes *et al.*, 1995), we might expect to find that increased scavenging and aggregation processes may lead to a large number of trapped particles inside ice crystals. Air bubbles may also be trapped inside rapidly growing ice particles or inside suddenly frozen supercooled water droplets. Furthermore, particle growth by riming also leads to highly inhomogeneous internal structures.

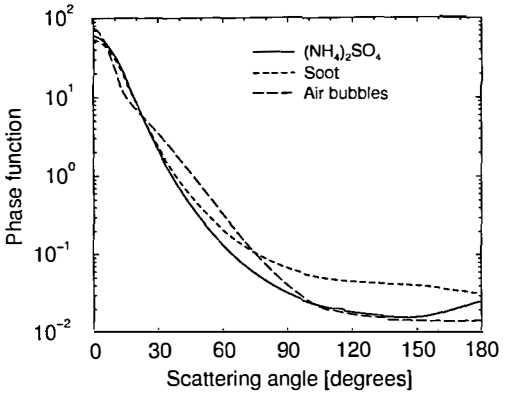

Figure 2 Scattering phase functions of spherical inclusions made of ammonium sulfate, soot, and air bubbles embedded in a hexagonal ice crystal. Reprinted from A. Macke, M. I. Mishchenko, and B. Cairns (1996a), The influence of inclusions on light scattering by large ice particles. J. Geophys. Res. **101**, 23,311–23,316; © 1996 by the American Geophysical Union.

Three types of internal scatterers are considered here: ammonium sulfate aerosols [$(NH_4)_2SO_4$], soot particles, and air bubbles. Figure 2 shows the scattering phase functions for these types of internal scatterers. Both ammonium sulfate particles and air bubbles are transparent in the visible. Therefore, these particles only affect the scattering properties of the ice crystal scattering phase function. Soot, on the other hand, is strongly absorbing and, therefore, has the potential of increasing the ice particles' absorption. The sizes of all types of impurities are assumed to obey a standard gamma distribution defined by an effective radius r_{eff} and an effective variance v_{eff} (Hansen and Travis, 1974). The values chosen for the three scatterers are given in Table I. The refractive indices $m = m_r + im_i$ are taken from Toon *et al.* (1976) for $(NH_4)_2SO_4$ and from Nilsson (1979) for soot. For air bubbles m is set to 1. These values are divided by the refractive index of ice (Warren, 1984), for which the small imaginary part ($\sim 10^{-9}$) is neglected, to obtain the respective relative refractive indices (Table I). Because the impurities are assumed to be spherical, the Lorenz–Mie theory was used to obtain the size-distributionally averaged optical properties of the internal scatterers relative to the surrounding ice material. Calculations were performed at a wavelength of $\lambda = 0.55$ μm, corresponding to maximum solar irradiation. The resulting extinction efficiencies $Q_{\text{ext}}(\text{incl}) = C_{\text{ext}}(\text{incl})/(\text{average projected area})$, single-scattering albedo ϖ_{incl}, and asymmetry parameters $\langle \cos \Theta \rangle_{\text{incl}}$ are shown in Table I. Figure 2 compares the phase functions of the internal scatterers.

The number density of the inclusions determines the mean free path length $\bar{l}$ [Eq. (1)] or, equivalently, the volume extinction coefficient $k_{\text{ext}} = 1/\bar{l}$. For an

Table I

Effective Radius r_{eff} and Effective Variance v_{eff} for Three Types of Inclusions, Inclusion Relative Refractive Indices (m_r, m_i), and Respective Size-Averaged Extinction Efficiencies Q_{ext}(incl), Single-Scattering Albedos ϖ_{incl}, and Asymmetry Parameters $\langle\cos\Theta\rangle_{\text{incl}}$

Type	r_{eff} (μm)	v_{eff}	(m_r, m_i)	Q_{ext}(incl)	ϖ_{incl}	$\langle\cos\Theta\rangle_{\text{incl}}$
$(NH_4)_2SO_4$	0.5	0.2	(1.15, 0.0)	1.354	1.0000	0.9213
Soot	0.5	0.2	(1.18, 0.38)	2.122	0.4257	0.9033
Air bubbles	1.0	0.1	(0.75, 0.0)	1.977	1.0000	0.8817

Source: A. Macke, M. I. Mishchenko, and B. Cairns (1997), The influence of inclusions on light scattering by large hexagonal and spherical ice crystals, *in* "IRS'96 Current Problems in Atmospheric Radiation" (W. L. Smith and K. Stamnes, Eds.), pp. 226–229, Deepak, Hampton, VA.

ensemble of n_0 particles per unit volume element with sizes obeying the standard gamma distribution, k_{ext} is given by (Lacis and Mishchenko, 1995)

$$k_{\text{ext}} = \pi r_{\text{eff}}^2 (1 - v_{\text{eff}})(1 - 2v_{\text{eff}}) Q_{\text{ext}} n_0. \tag{11}$$

It is often more convenient to describe the optical density of the inclusions in terms of the optical thickness τ. To this end, the volume extinction coefficient must be multiplied by a length H, which represents a characteristic dimension of the host particle. For the purpose of this study, H is defined by the maximum dimension of the host particle. However, it should be noted that this choice does not necessarily reflect the typical length scale for spherical and nonspherical particles. See Macke *et al.* (1996a) for a brief discussion of this problem.

The effects of different types of internal impurities are studied for a hexagonal ice column with shape defined by a length to (hexagonal) diameter ratio of 200 μm/100 μm. This choice roughly corresponds to the mean particle dimensions observed in natural cirrus clouds.

Figure 3 shows the total scattering phase function (ice column with inclusions) for optical thicknesses $\tau = 0.5$, 2.5, and 5. With increasing τ, all three inclusions cause a noticeable broadening of the forward scattering features from 0° to 22°, as well as a decrease in the magnitude of the 22° halo maximum. The broadening results from the predominantly forward scattering phase functions of the individual impurities, which spreads the light rays that are directly transmitted through plane-parallel crystal facets. The same mechanism reduces the magnitude of the halos and the magnitude of the backscattering peak. The nonabsorbing inclusions cause an increase in side scattering, whereas side scattering decreases in magnitude for ice crystals containing soot particles. For both absorbing and nonabsorb-

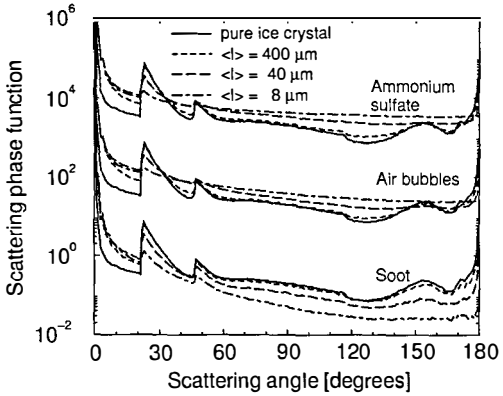

Figure 3 Scattering phase functions of a hexagonal column with internal ammonium sulfate (multiplied by 10^4), air bubble (multiplied by 10^2), and soot inclusions. The optical thickness of the internal scatterers is τ = 0.5, 2.5, and 5. Reprinted with changes from A. Macke, M. I. Mishchenko, and B. Cairns (1996a), The influence of inclusions on light scattering by large ice particles. J. Geophys. Res. **101**, 23,311–23,316; © 1996 by the American Geophysical Union.

ing inclusions, the departures from the scattering phase function for the pure ice crystal increases as the inclusion number density increases. However, additional absorption caused by soot particles reduces the contribution of refracted rays to the total phase function [Eq. (8)], which explains the opposite side scattering effects for ice particles with absorbing versus nonabsorbing contaminations.

Ice particles in the atmosphere are often quite irregular in shape rather than a simple crystal and thus the assumption of symmetric hexagonal particles is not valid in this case. In this regard, an interesting question is whether internal scatterers significantly change the overall scattering properties of an irregularly shaped host particle, which has no characteristic ray paths because of its randomized geometry. Figure 4 shows the scattering phase functions of a randomized, fractal-type host particle (see Macke *et al.*, 1996b, for details) with increasing optical thickness of air bubble inclusions. A comparison with Fig. 3 indeed reveals that the inclusions have a weaker effect on the overall scattering properties for more irregularly shaped particles. However, the changes in the total scattering phase function are still significant, even for optical thicknesses as small as 0.5. Unlike the situation for a hexagonal host particle, internal scattering in the random polycrystal leads to a sharper forward scattering pattern. This result may be explained by the fact that the forward scattering for a homogeneous polycrystal is determined by a superposition of halos resulting from a minimum deviation for various component ice prisms, whereas internal scattering processes complicate the conditions for this minimum deviation and apparently increase the fraction of

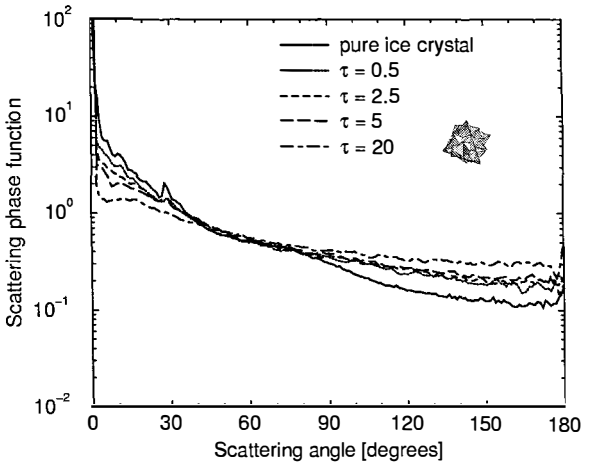

Figure 4 Phase function versus scattering angle for a random polycrystal with increasing optical thickness of air bubble inclusions.

internal reflections at the expense of direct transmissions. We note that this random polycrystal with air bubble inclusions may serve as a model for graupel and hailstone particles, which possess irregular external geometries as well as internal inhomogeneities in the form of air bubble inclusions (e.g., Pruppacher and Klett, 1997).

B. Planetary Regolith Particles

Because large, homogeneous particles always have positive asymmetry parameters, it has been hypothesized that the negative asymmetry parameters of planetary regolith particles retrieved with an approximate bidirectional reflectance model (Hapke, 1993) result from their presumably complicated internal structure. The diameter of lunar regolith particles is typically about 50 μm, so that scattering of visible light by such particles can be described by means of the geometric optics approximation.

In the following, spherical host particles with a diameter of 50 μm and refractive indices at $\lambda = 0.55$ μm equal to 1.55 and 1.31 are assumed, corresponding to silicate and pure ice, respectively. Both materials commonly cover surfaces of bodies in the solar system. For the scattering inclusions, refractive indices are chosen to represent either voids inside the host particle ($m = 1$) or refractive grains with large and small contrast compared to the host particle ($m = 2$, $m = 1.65$). Table II shows the four types of host/inclusion pairs used in this study.

Table II

Refractive Indices of the Host Medium and Inclusions

Type	m_{host}	m_{incl}
1	1.55	1
2	1.55	2
3	1.55	1.65
4	1.31	1

Source: M. I. Mishchenko and A. Macke (1997), Asymetry parameters of the phase function for isolated and densely packed spherical particles with multiple internal inclusions in the geometric optics limit, *J. Quant. Spectrosc. Radiat. Transfer* **57**, 767–794.

The size distribution of the inclusions is assumed to follow the standard gamma distribution (Hansen and Travis, 1974) with an effective radius of 0.5 μm and an effective variance of 0.1. The single-scattering properties of the inclusions have been calculated using the Lorenz–Mie theory. Figure 5 shows the corresponding scattering phase functions.

Equation (10), which assumes $\langle \cos\Theta \rangle^{\text{D}} \approx 1$, already suggests that the total asymmetry parameter for a large, isolated, composite particle cannot be negative. The only way to make the total asymmetry parameter equal to 0 is to have only nonabsorbing inclusions and a backward delta-function-like ray-tracing phase function, so that $\varpi^{\text{RT}} = 1$ and $\langle \cos\Theta \rangle^{\text{RT}} = -1$. In fact, Fig. 6 shows that the ray-tracing asymmetry parameter $\langle \cos\Theta \rangle^{\text{RT}}$ for the nonabsorbing composite particle does decrease systematically with increasing optical thickness. However, in none of the cases does it approach -1 or even become noticeably smaller than 0. The smallest $\langle \cos\Theta \rangle^{\text{RT}}$ value is equal to -0.0122 and corresponds to the type 1 composite particle and an extremely large optical thickness of $\tau = 25$. As a consequence, the total asymmetry parameter values are always positive and never drop below 0.4922.

It has been suggested by Hapke (1993) that the ray-tracing asymmetry parameter can be reduced significantly by increasing absorption inside the composite particle because in this case it is only the light scattered to the sides and rear by the inclusions near the back-facing surface of the composite particle that readily escapes. However, because the inclusions scatter light predominantly in the forward direction (Fig. 5), backscattering by the composite particle requires (multiple) internal scattering events and thus longer ray paths than the direct transmittance that causes the forward scattering. Therefore, increasing absorption suppresses the backscattering component of the ray-tracing phase function. Furthermore, it

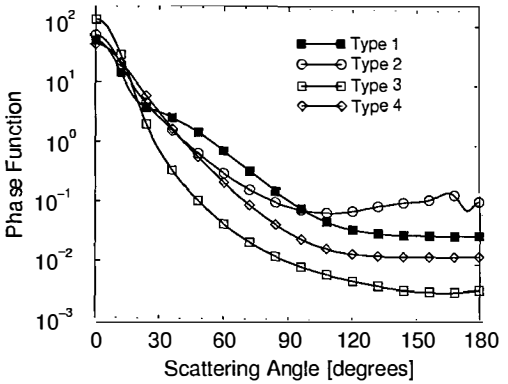

Figure 5 Phase function versus scattering angle for four types of internal inclusions. Reprinted from M. I. Mishchenko and A. Macke (1997), Assymetry parameters of the phase function for isolated and densely packed spherical particles with multiple internal inclusions in the geometric optics limit, *J. Quant. Spectrosc. Radiat. Transfer* **57**, 767–794, © 1997, with permission from Elsevier Science.

follows from Eq. (9) that increasing absorption reduces the ray-tracing contribution to the total asymmetry parameter so that the strongly forward scattering diffraction component dominates, and the asymmetry parameter of the composite particle increases. Therefore, the only way to considerably reduce the ray-tracing

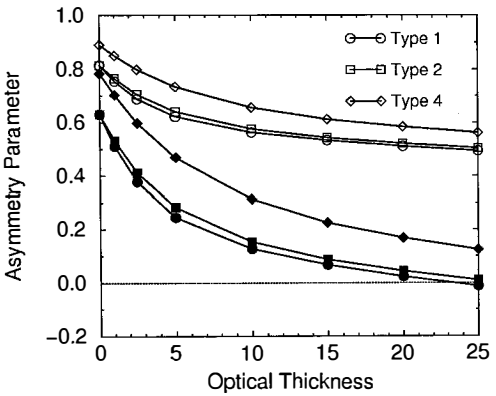

Figure 6 Ray-tracing (filled symbols) and total (open symbols) asymmetry parameters versus scattering optical thickness τ for type 1, type 2, and type 4 composite particles. Reprinted from M. I. Mishchenko and A. Macke (1997), Assymetry parameters of the phase function for isolated and densely packed spherical particles with multiple internal inclusions in the geometric optics limit, *J. Quant. Spectrosc. Radiat. Transfer* **57**, 767–794, © 1997, with permission from Elsevier Science.

asymmetry parameter is to increase the amount of multiple scattering inside the composite particle. This can only be achieved by decreasing rather than by increasing the absorption.

Similar calculations for the type 3 composite particle show that the reduced contrast between the inclusions and the host medium causes significantly larger ray-tracing asymmetry parameters than for the type 1 and type 2 particles. This readily can be explained by the fact that the type 3 inclusion has a stronger forward scattering and a weaker backscattering component than the phase functions for the type 1 and type 2 inclusions (Fig. 5).

Figure 6 shows that the ray-tracing asymmetry parameter for the composite ice particle (type 4) is systematically larger than that for silicate particles. This can be explained by the fact that the phase function for vacuum bubbles in ice is less backscattering than that for both vacuum bubbles and highly refractive grains in the silicate host medium (Fig. 5). Furthermore, homogeneous particles with a lower refractive index (ice) tend to be more forward scattering than those with a larger refractive index (silicate). It thus appears that it is more difficult to make an ice particle backscattering by filling it with multiple voids than it is for a silicate particle.

The qualitative results of this section also hold for densely packed large composite particles, even for isotropic scattering internal inclusions. A detailed discussion can be found in Mishchenko and Macke (1997) and Hillier (1997).

IV. ANALYTIC APPROXIMATION

From the practical point of view, it is interesting to compare RT/MC results with those obtained by an independent scattering approximation (ISA), where the scattering properties of the host particle and the inclusions are treated separately, that is, where radiative interactions between the ice particle surface and the embedded inclusions are neglected. Note that the ISA still requires that the refractive indices of the inclusions have to be given with respect to the refractive index of the host particle.

Because the internal scatterers do not affect the diffraction pattern of the host particle, only the ray-tracing phase function needs to be modified. The composite ray-tracing phase function of the homogeneous host particle and the inclusions is given by

$$a_1^{\mathrm{RT}}(\mathrm{host}+\mathrm{incl}) = \frac{C_{\mathrm{sca}}^{\mathrm{RT}}(\mathrm{host})a_1^{\mathrm{RT}}(\mathrm{host}) + NC_{\mathrm{sca}}(\mathrm{incl})a_1^{\mathrm{incl}}}{C_{\mathrm{sca}}^{\mathrm{RT}}(\mathrm{host}) + NC_{\mathrm{sca}}(\mathrm{incl})}. \qquad (12)$$

Here, $C_{\mathrm{sca}}^{\mathrm{RT}}(\mathrm{host})$ and $a_1^{\mathrm{RT}}(\mathrm{host})$ denote the scattering cross section and the ray-tracing phase function of the homogeneous host particle. The number, scattering

Table III

Asymmetry Parameter $\langle\cos\Theta\rangle$ for Ice Crystals Containing Ammonium Sulfate, Air Bubble, and Soot Inclusions as a Function of τ (See Text). The Changes in the Single-Scattering Albedo ϖ for Crystals with (Absorbing) Soot Inclusions are Also Shown. Results Based on the Independent Scattering Approximation are Given in Parentheses

τ	$\langle\cos\Theta\rangle$, $(NH_4)_2SO_4$	$\langle\cos\Theta\rangle$, air bubbles	$\langle\cos\Theta\rangle$, soot	ϖ, soot
0	0.8153	0.8153	0.8153	1.0000
0.5	0.8113 (0.8370)	0.8060 (0.8340)	0.8372 (0.8484)	0.9249 (0.9307)
2.5	0.7841 (0.8832)	0.7722 (0.8740)	0.8905 (0.9253)	0.7128 (0.7372)
5	0.7588 (0.9079)	0.7385 (0.8953)	0.9233 (0.9686)	0.5906 (0.6125)
10	0.7215 (0.9284)	0.6935 (0.9131)	0.9512 (0.9945)	0.5164 (0.5253)

Source: A. Macke, M. I. Mishchenko, and B. Cairns (1997), The influence of inclusions on light scattering by large hexagonal and spherical ice crystals, *in* "IRS'96 Current Problems in Atmospheric Radiation" (W. L. Smith and K. Stamnes, Eds.), pp. 226–229, Deepak, Hampton, VA.

cross section, and scattering phase function of the inclusions are represented by N, $C_{\rm sca}(\text{incl})$, and $a_1^{\rm incl}$.

Similarly, adding the single-scattering albedo of the host and the inclusions yields

$$\varpi^{\rm RT}(\text{host}+\text{incl}) = \frac{C_{\rm sca}^{\rm RT}(\text{host}) + NC_{\rm sca}(\text{incl})}{C_{\rm ext}^{\rm RT}(\text{host}) + NC_{\rm ext}(\text{incl})} = \frac{C_{\rm ext}^{\rm RT}(\text{host})\varpi_{\rm host}^{\rm RT} + NC_{\rm ext}(\text{incl})\varpi_{\rm incl}}{C_{\rm ext}^{\rm RT}(\text{host}) + NC_{\rm ext}(\text{incl})}. \tag{13}$$

Substituting Eqs. (12) and (13) into Eq. (8) provides the total phase function of the host/inclusions combination in the approximation of independent scattering.

Table III shows the approximate asymmetry parameter and single-scattering albedo (the latter, for soot only) together with the RT/MC results for a hexagonal host particle as discussed in Section III.A. The ISA results are given in parentheses. Obviously, the ISA does not give a satisfactory estimate of the true scattering behavior, even for internal scatterers with small optical thickness. For the nonabsorbing inclusions, $\langle\cos\Theta\rangle$ increases with increasing τ, contrary to the RT/MC results. An independent superposition of the phase functions of the ice crystal and inclusions mostly affects the forward scattering region, while side and backscattering are little influenced because both constituents are already predominantly forward scattering. As a result, the combined forward scattering peak becomes broader, the side scattering and backscattering remain almost the same, and the asymmetry parameter increases. On the other hand, a change in the internal ray

paths as simulated in the Monte Carlo procedure not only influences the forward scattering behavior, but also all subsequent internal reflections, thereby leading to a broadening of the forward scattering peak and a systematic increase in side scattering and backscattering. In other words, scattering by the host particle and the internal inclusions is strongly coupled because of the ability of the inclusions to systematically change the internal ray paths. In case of absorption either by the ice crystal or by the inclusions, the length of the effective ray paths and, thus, the coupling decreases. This is demonstrated by the case of soot inclusions, for which the RT/MC and ISA results agree better than for nonabsorbing inclusions.

V. CONCLUSIONS

The demonstrated influence of different types of inclusions on the single-scattering behavior of a composite particle provides an additional motivation for studying the internal structures of naturally occurring particles. A more accurate characterization of the impurity effects requires a more precise knowledge of realistic number densities and of inclusion sizes.

Although the present study assumes uniformly distributed inclusions, it should be noted that the Monte Carlo technique applied can be easily extended to nonuniform distributions of internal scatterers.

Finally, natural inclusions are not always spherical in shape, thereby potentially preventing the use of the Lorenz–Mie theory to solve for their single-scattering properties. Therefore, future applications of the RT/MC technique should take advantage of results from scattering theories such as the T-matrix method (Mishchenko, 1993; Chapter 6), the finite difference time domain method (Yang and Liou, 1995; Chapter 7), or the discrete dipole approximation (Draine and Flatau, 1994; Chapter 5), which are suitable for nonspherical particle shapes.

A standard Fortran 90 implementation of the RT/MC technique is freely available from the author upon request.

ACKNOWLEDGMENT

The author is grateful to M. Mishchenko for valuable discussions and substantial motivations to the work presented in Section III.B.